Temperature-dependent clear-sky feedbacks in radiative-convective equilibrium

Lukas Kluft[1], Sally Dacie[1], Manfred Brath[2], Stefan Alexander Buehler[2], and Bjorn Stevens[1]

[1]Max Planck Institute for Meteorology
[2]Universität Hamburg

November 21, 2022

Abstract

We quantify the temperature-dependence of clear-sky radiative feedbacks in a tropical radiative-convective equilibrium model. The longwave radiative fluxes are computed using a line-by-line radiative transfer model to ensure accuracy in very warm and moist climates. The one-dimensional model is tuned to surface temperatures between 285 and 313 K by modifying a surface enthalpy sink, which does not directly interfere with radiative fluxes in the atmosphere. The total climate feedback increases from -1.7 to -0.8 Wmˆ-2Kˆ-1 for surface temperatures up to 305 K due to a strengthening of the water-vapor feedback. The temperature-dependence maximizes at surface temperatures around 297 K, which is close to the present-day tropical mean temperature.

At surface temperatures above 305 K, the atmosphere becomes fully opaque and the radiative feedback is almost constant.
This near-constancy is in agreement with a theoretical model of the water-vapor feedback presented by Ingram (2010), but in disagreement with other modeling studies.

Temperature-dependent clear-sky feedbacks in radiative-convective equilibrium

Lukas Kluft[1,2,3], Sally Dacie[1,2], Manfred Brath[3], Stefan A. Buehler[3], and Bjorn Stevens[1]

[1]Max Planck Institute for Meteorology

[2]International Max Planck Research School for Earth System Modeling

[3] Meteorologisches Institut, Centrum für Erdsystem- und Nachhaltigkeitsforschung (CEN), Fachbereich Geowissenschaften, Universität Hamburg

Key Points:

- State-dependence of clear-sky feedbacks maximizes at temperatures around 295 K, when the atmospheric emission window closes
- Away from this temperature regime the temperature dependence is weak
- RRTMG becomes inaccurate at surface temperatures above 308 K, line-by-line calculations show no evidence of a clear-sky runaway greenhouse

Corresponding author: Lukas Kluft, `lukas.kluft@mpimet.mpg.de`

Abstract

We quantify the temperature-dependence of clear-sky radiative feedbacks in a tropical radiative-convective equilibrium model. The longwave radiative fluxes are computed using a line-by-line radiative transfer model to ensure accuracy in very warm and moist climates. The one-dimensional model is tuned to surface temperatures between 285 and 313 K by modifying a surface enthalpy sink, which does not directly interfere with radiative fluxes in the atmosphere. The total climate feedback increases from -1.7 to $-0.8\,\mathrm{Wm^{-2}K^{-1}}$ for surface temperatures up to 305 K due to a strengthening of the water-vapor feedback. The temperature-dependence maximizes at surface temperatures around 297 K, which is close to the present-day tropical mean temperature. At surface temperatures above 305 K, the atmosphere becomes fully opaque and the radiative feedback is almost constant. This near-constancy is in agreement with a theoretical model of the water-vapor feedback presented by Ingram (2010), but in disagreement with other modeling studies.

Plain Language Summary

Climate sensitivity, the change in surface temperature in response to a doubling of atmospheric CO_2, is one of the most important quantities when discussing climate change. Our current understanding is that this surface warming depends on the current state of the climate system.

We analyze how temperature affects the climate sensitivity by running a simple climate model at different surface temperatures. We find that the climate sensitivity is stronger at warmer temperatures, i.e. that a warmer climate system warms more, in agreement with other climate models. However, we find that this temperature-dependence vanishes at temperatures above 305 K (32°C). While previous modeling studies did not find this behavior because of their simplified representation of radiative processes in the atmosphere, our findings are consistent with a conceptual model of climate sensitivity.

1 Introduction

The state-dependence of the climate feedback, that is its change with surface temperature, is of great interest when studying climate change. It has to be taken into account when comparing global climate models among each other or with historical observations. Although recent work focuses on changes to cloud feedbacks due to changes in self-aggregation, cloud amount, or cloud height (Cronin & Wing, 2017; Hohenegger & Stevens, 2016; Becker & Stevens, 2014), there is also discussion about a temperature-dependence to the more fundamental clear-sky radiative feedbacks.

Meraner et al. (2013) find a robust increase of the climate feedback by analyzing an ensemble of artificial atmosphere profiles covering surface temperatures from 280 to 310 K. They attribute changes to a strengthening of the water-vapor feedback. This is in line with the work of Koll and Cronin (2018), who analyzed changes in the spectral outgoing longwave radiation. They found a closing of the atmospheric emission window due to increased continuum absorption caused by the abundance of water vapor at higher temperatures. Romps (2020) used a cloud-resolving model to run simulations for a vast range of surface temperatures to find the corresponding equilibrium CO_2 concentrations. They confirm the increase of the climate feedback with temperature up to 308 K; at higher surface temperatures they find a decrease of the climate feedback estimates.

In Kluft et al. (2019), we analyzed changes of clear-sky radiative feedbacks in a one-dimensional radiative-convective equilibrium (RCE) model by consecutive doublings of the CO_2 concentration between 0.5 to 8 times a reference concentration. This study was the first to compare the response of RCE using offline line-by-line radiative transfer calculations. They agreed well with the fast radiation scheme RRTMG (Mlawer et al., 1997) in the temperature regimes examined, as well as allowing us to gain insight into the spectral dependence of the clear-sky feedbacks.

Because there is no evidence that RRTMG is valid over such a wide range of temperatures and good reason to think it might not be, we here replace the longwave component of the radiative transfer scheme with the line-by-line model ARTS. In contrast to Kluft et al. (2019) the line-by-line model is used online to calculate the heating rates used to force the RCE model.

We sample a wide range of surface temperatures by introducing a surface enthalpy sink. We argue that this method is best suited to analyze state-dependencies, as it does not affect the radiative balance in ways other than by changing the surface temperature, which is intended. This, and the use of line-by-line radiative transfer, allows us to push the model to higher temperatures — outside of the range where commonly used radiative transfer schemes have been validated, and where past studies hinted at a runaway greenhouse effect.

2 Tuning the model to different climate states

To analyze temperature-dependencies the observed climate model needs to be tuned to different equilibrated initial states. In principle, this can be achieved by changing any boundary condition of the system, like the solar constant or the surface albedo. For simpler models, like 1D-RCE, it is also possible to modify the relative humidity distribution. However, this raises the intrinsic problem that it is no longer obvious if changes in a quantity result from the modified state or the modified boundary condition itself. We will illustrate this by discussing modifications of the solar constant, the relative humidity, and the poleward enthalpy transport.

Adjusting the solar constant is a straight-forward approach to tune the surface temperature of an RCE model. This method has a long history for many types of climate models (Budyko, 1969). Using this technique it is possible to cover a wide range of surface temperatures. However, a reduction in insolation has an impact on the shortwave fluxes and the derived shortwave heating rates. The shortwave heating directly controls the stratospheric temperature profile, which is in a pure radiative equilibrium.

Another way to tune the surface temperature is to adjust the relative humidity: Decreasing the amount of water vapor at a given temperature allows more radiation to be emitted into space, which reduces the simulated surface temperature. We used this method in Kluft et al. (2019) to simulate tropical surface temperatures while keeping the sun-geometry and solar constant at global mean values. However, tuning the relative humidity modulates the strength of the water-vapor feedback as it limits the absolute amount of atmospheric water vapor at a given temperature.

We here pursue a third option to simulate different surface temperature states in an RCE model, namely adding a surface enthalpy sink (Drotos et al., 2020; Hohenegger & Stevens, 2016; Becker & Stevens, 2014). From the global zonal mean radiation budget we know that there is very significant export of heat from the tropics to the extra-tropics by the atmosphere and ocean circulations (Niiler, 1992). Modeling studies suggest that it is strong enough to balance the increased insolation in the tropics compared to the extra-tropics, which results in a net energy uptake close to the global mean insolation (Popke et al., 2013). For simplicity, we assume that all the heat transport takes place in the ocean. The ocean enthalpy sink is implemented by accounting for an offset when deriving the surface heating from the energy budget:

$$\frac{\partial T_\mathrm{s}}{\partial t} = \frac{\Delta F_\mathrm{rad} + F_\mathrm{con} + F_\mathrm{s}}{C_\mathrm{s}} \tag{1}$$

with surface temperature T_s, net radiative fluxes at the surface ΔF_rad, convective flux F_con, surface heat capacity C_s, and ocean enthalpy sink F_s.

The temperature-dependence of the radiative feedback can be studied by using different values for F_s. Changing F_s changes the outgoing longwave radiation through the surface temperature only, but does not directly affect other radiative quantities. This is a decisive advantage compared to the tuning methods mentioned earlier. From the point of view of radiative fluxes, this method is very similar to fixing the surface temperature at given values and comparing the outgoing longwave radiation (Meraner et al., 2013). Both methods result in a non-zero net radiation at the top of the atmosphere. However by specifying F_s to achieve a desired surface temperature one explicitly models the surface equilibration, consistent with an assumed ocean heat capacity, thus preserving the time-scales of the adjustment process (Cronin & Emanuel, 2013).

3 Model configuration

The simulations in this study have been performed using the RCE model konrad (Kluft & Dacie, 2020, v0.8.0), which is developed under the MIT License and is freely available on `github.com/atmtools/konrad`.

We replace the longwave component of the radiation scheme with the line-by-line radiative transfer model ARTS (Buehler et al., 2018; Eriksson et al., 2011). ARTS is used to calculate the longwave radiative fluxes based on 32,768 equidistant frequency points between 10–3,250 $\mathrm{cm^{-1}}$. Gas absorption is based on the HITRAN database (Gordon et al., 2017) and the MT_CKD model for the continuum absorption of water vapor, CO_2, and molecular nitrogen (Mlawer et al., 2012, Version 2.52).

3.1 Boundary conditions

The boundary conditions are following Kluft et al. (2019) in general: The reference CO_2 concentration is 348 ppmv and the surface albedo is set to 0.2 to account for some reflection by clouds, that are not included in our clear-sky model. We have decreased the ocean depth to 1 m to accelerate the simulations and compensate for the increased computational cost due to the line-by-line radiative transfer.

There are some modifications to more closely represent the tropical atmosphere. The solar constant is set to $551.58\,\mathrm{W m^{-2}}$ at an zenith angle of 42.05° resulting in an insolation of $409.6\,\mathrm{W m^{-2}}$ (Wing et al., 2017; Cronin, 2014). The relative humidity in the troposphere is set to 80 % up to the cold-point tropopause above which the volume mixing ratio is kept constant. This ensures a reasonable amount of humidity in the upper troposphere, which is key for the interaction of lapse-rate and water-vapor feedbacks (Minschwaner & Dessler, 2004; Kluft et al., 2019).

We introduce an enthalpy sink in the ocean mixed layer, which we imagine as a poleward ocean enthalpy transport, which allows our model to be tuned to virtually any surface temperature. A surface heat transport F_s of $-66\,\mathrm{W m^{-2}}$ results in a net energy influx that is equal to the global mean of around $343\,\mathrm{W m^{-2}}$ and a surface temperature of 298 K in agreement with a GCM study by Popke et al. (2013).

3.2 Treatment of ozone

Konrad does not include atmospheric chemistry, hence atmospheric trace gases are represented as vertical profiles of volume mixing ratios that do not change with time. This assumption is reasonable for most trace gases, especially if the atmospheric state does not deviate much from the present-day climate.

The latter assumption, however, is not valid when simulating atmospheres with much warmer surface temperatures than currently observed. The expansion of the troposphere in a warming climate in combination with an ozone profile that is fixed on pressure levels causes high ozone concentrations in the upper troposphere. In the real atmosphere, chemical depletion acts as a ozone sink in the troposphere.

If this is not taken into account, a fixed ozone profile acts as a “temperature ramp” for the tropopause and leads to an unreasonable increase of tropopause temperatures in a warming climate (Dacie et al., 2019). A fixed prescribed ozone profile leads to a runaway in our simulations, when temperatures exceed 300 K (not shown). This runaway is most likely caused by the unphysical high ozone concentrations in the upper troposphere.

Therefore, we couple the ozone profile to a reference level in the atmospheric temperature profile, which we have chosen to be the cold-point tropopause. When this reference level changes its altitude the ozone profile is shifted by the same amount in logarithmic pressure coordinates.

3.3 Reference climate

Figure 1 shows the temperature profiles for two RCE configurations as well as a climatology based on tropical ocean profiles (30°S–30°N) from ERA5 from January 2008 to May 2018. The new tropical configuration (teal) leads to an improved representation of the shape of the tropical tropopause in comparison to Kluft et al. (2019, grey). This can be attributed to both an increased insolation which warms the stratosphere around the ozone layer, as well as an increased longwave cooling around the cold point due to a higher water vapor content.

In summary, the modified model configuration better represents the tropical mean atmosphere (boundary conditions) and allows accurate studies of clear-sky radiative feedbacks for a wide range of surface temperatures (line-by-line radiation).

Our model does not include some of the features known to influence the state of the observed tropical atmosphere, for instance clouds, or variations of humidity, both of which have spatial variability linked to tropical circulation systems. Nonetheless we believe the insights derived from our study are informative about the actual atmosphere, and about more complex models used to study it.

4 Radiative feedbacks

4.1 Decomposed climate feedbacks

We want to quantify the (surface) temperature-dependence for different radiative clear-sky feedbacks. Following Gregory et al. (2004), let us take the radiative feedback parameter λ from the linear regression of the top-of-the-atmosphere radiative imbalance ΔF_{TOA} against the surface temperature change ΔT_{s}:

$$\lambda = -\frac{\Delta F_{\mathrm{TOA}}}{\Delta T_{\mathrm{s}}} \tag{2}$$

The linear regression is performed after the stratosphere has adjusted to the instantaneous forcing by only using values 30 days after the radiative imbalance reaches its max-

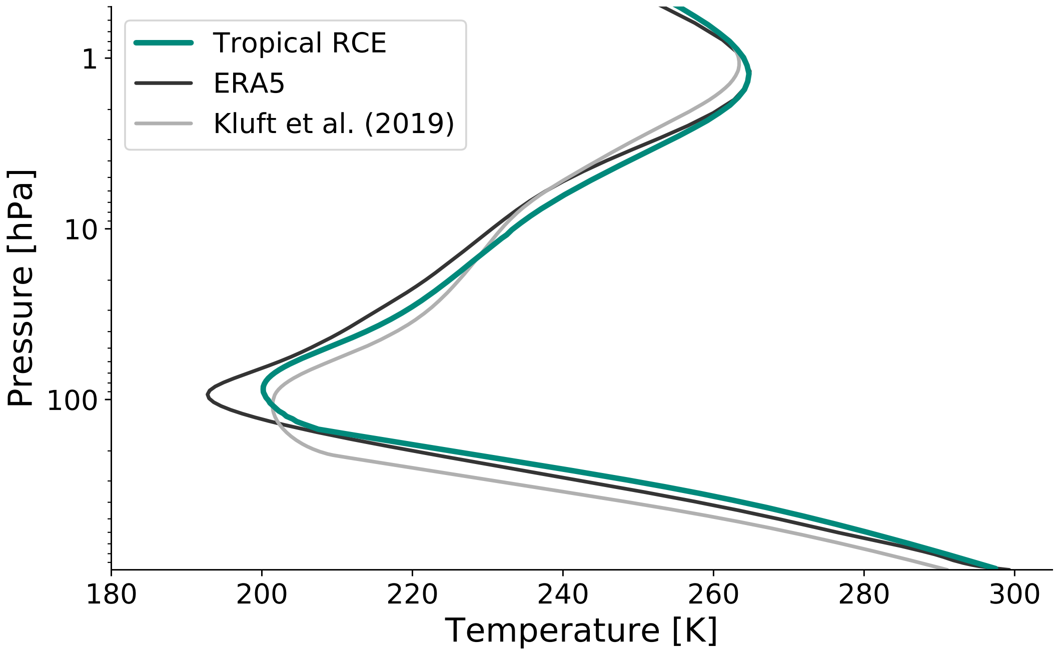

Figure 1. Equilibrium temperature profile as a function of atmospheric pressure for an RCE with global insolation (Kluft et al., 2019, grey), our tropical configuration (teal), and a tropical reanalysis (black). The figure is clipped at 0.5 hPa to better visualize the troposphere.

imum (Gregory plots for different surface temperatures are shown in the supporting information).

Following Kluft et al. (2019) the total radiative feedback is decomposed into its components, the Planck λ_{PL}, the water-vapor λ_{WV}, the lapse rate λ_{LR}, and an additional water-vapor–lapse-rate feedback $\lambda_{\mathrm{WV}\wedge\mathrm{LR}}$ by using separate model runs in which individual feedback mechanisms are selectively turned on or off.

The only exception from this calculation is the Planck feedback. The simplest model configuration, which is used to determine the Planck feedback, still has a coupled ozone profile. In combination with a discrete vertical grid, this can lead to small differences in how model runs react to a given radiative forcing. These differences propagate through the whole feedback decomposition, because the Planck feedback is subtracted from every other radiative feedback. Therefore, we are using an analytical model to determine the Planck feedback based on the boundary conditions of our model.

In general, the Planck feedback λ_{PL} is defined as the response of the outgoing longwave radiation J to changes in the surface temperature T_{s}. For a black-body, J is described by the Stefan-Boltzmann law

$$J = \sigma T^4 \tag{3}$$

with Stefan-Boltzmann constant σ and temperature T. For the Earth's atmosphere, the Planck feedback λ_{PL} can be approximated using the temperature derivative of the Stefan-Boltzmann law but using the effective temperature T_ϵ:

$$-\lambda_{\mathrm{PL}} = \frac{\partial J}{\partial T} \approx 4\sigma T_\epsilon^3 \tag{4}$$

The effective temperature of the climate system T_ϵ is defined as the temperature of a black-body that would emit the same amount of radiation. In equilibrium, T_ϵ is constrained by the net amount of shortwave radiation that enters the system, and can be computed by again using the Stefan-Boltzmann law:

$$T_\epsilon = \sqrt[4]{\frac{(1-\alpha)\cdot S_0 \cdot \cos(\theta) - F_{\mathrm{s}}}{\sigma}} \tag{5}$$

with surface albedo $\alpha = 0.2$, solar constant $S_0 = 551.58\,\mathrm{Wm^{-2}}$, solar zenith angle $\theta = 42.05°$, and ocean enthalpy sink F_{s}. By using Equation 4 and 5 we are able to compute the Planck feedback for the boundary conditions of each ensemble member.

Konrad is run with different values of the surface enthalpy sink ranging from -52 to $-82\,\mathrm{Wm^{-2}}$, which results in surface temperatures between 313 K and 285 K. After euqilibrating to the initial conditions, every model configuration is forced with a doubling of the CO_2 concentration. Figure 2a shows the strength of the individual radiative feedbacks as a function of the initial surface temperature. In addition, a cubic spline is fitted for every individual feedback (solid lines) to estimate its temperature-dependence, i.e. $\partial\lambda/\partial T_{\mathrm{s}}$ (shown in Figure 2b).

The magnitude of the water-vapor (blue) and lapse-rate (red) feedbacks are larger than in Kluft et al. (2019). This difference can be attributed to the modified model configuration and, on its own, is evidence of a state-dependent climate feedback.

The water-vapor feedback (blue) increases from 2.3 to $3.7\,\mathrm{Wm^{-2}K^{-1}}$ with increasing surface temperature. Meraner et al. (2013) find a similar increase of the ECS in their RCE-like calculations, which they also attribute to changes in the water-vapor feedback. Koll and Cronin (2018) performed line-by-line radiative transfer calculations to show that this is mainly driven by rapidly increasing continuum absorption in the atmospheric window. We find the same increase of the water-vapor feedback for surface temperatures up to 305 K. At even higher surface temperatures, when the atmospheric window is fully opaque, the water-vapor feedback is almost constant.

The decreasing temperature lapse rate in a warmer climate (Manabe & Stouffer, 1980, Sec. 5) leads to a strengthening of the lapse-rate feedback (red) from -1.8 to -6.5 $\mathrm{Wm^{-2}K^{-1}}$. The increase of lapse-rate feedback is more than twice as large as that of the water-vapor feedback, but balanced by its self-induced moistening of the upper troposphere, the WV$\wedge$LR feedback (Colman & McAvaney, 2009; Minschwaner & Dessler, 2004; Kluft et al., 2019). The balancing of both feedbacks is robust for all simulated surface temperatures (compare LR and WV$\wedge$LR in Figure 2).

As a result, the total radiative feedback λ (grey) is dominated by the temperature-dependence of the water-vapor feedback and increases from -1.7 to $-0.8\,\mathrm{Wm^{-2}K^{-1}}$ for surface temperatures between 285 K and 308 K. For the same temperature range, Meraner et al. (2013) find a higher increase of from -2 to $-0.67\,\mathrm{Wm^{-2}K^{-1}}$ (estimated from their Figure 4). The strongest temperature-dependence is found for surface temperatures around 297 K (Figure 2b), which is about the present-day tropical mean temperature. We attribute this to a rapid closing of the atmospheric window due to absorption by the water-vapor self-continuum (Koll & Cronin, 2018).

? (?) quantified the mean clear-sky feedback for 16 cloud-resolving models in RCE configuration. Their estimate of $-0.8\,\mathrm{Wm^{-2}K^{-1}}$ is in perfect agreement with our estimate at comparable surface temperatures, which indicates a robustness of the tropical clear-sky feedbacks.

For surface temperatures above 305 K the total radiative feedback is almost constant. This behavior has been predicted by Ingram (2010) in a qualitative model of the atmospheric water-vapor feedback: When the atmosphere is cold and dry, emission from the surface escapes to space. This emission increases as surface temperature increases giving a negative (Planck) feedback. As the atmosphere warms, it becomes more moist and optically thick. Eventually, the atmospheric window closes and emission from the surface is irrelevant because it no longer reaches space. Then, as the atmosphere warms and moistens, the optical depth increases and the emission layer shifts upwards. The increase in optical depth is controlled by the equilibrium water vapor pressure, which is a function of temperature. Assuming that temperatures in the troposphere are set by a lapse rate that is also a function of temperature (approximately true for the moist adiabat), the optical depth is a function of temperature only. As a result, the emission layer shifts upwards approximately maintaining a fixed temperature. In this case, the amount of emission does not change and we have zero feedback irrespective of further atmospheric warming.

Though the qualitative model suggests a zero feedback, we find a non-zero total feedback in our simulations. Ingram (2010) assumes that water vapor is the only relevant greenhouse gas and that it becomes opaque in the entire spectrum. In our model other gases like CO_2 are included and emission from these gases as well as the surface (in parts of the spectrum that are not opaque) can also affect the total feedback. This allows the climate system to increase its emission at certain wavenumbers (Section 5) and maintain a negative total feedback.

4.2 Discussion of state-dependence at high temperatures

In general, we find a robust increase of the total climate feedback for temperatures between 285 and 305 K which is in agreement with modeling studies by Meraner et al. (2013) and Romps (2020). However, differences emerge at high surface temperatures. Both studies find a stronger increase of the total radiative feedback which is followed by a decrease (more negative) at surface temperatures above 308 K.

To understand these differences we repeated the simulations using the radiation scheme RRTMG, which has been used by the two studies, to compute both longwave and shortwave heating rates. Figure 3a shows the decomposed radiative feedbacks for konrad using RRTMG (dashed lines) versus those calculated using ARTS (solid lines). An estimate of the temperature-dependence when using RRTMG is shown in the supporting information.

When using RRTMG the total feedback changes about 79 % from -1.72 to $-0.36\,\mathrm{Wm^{-2}K^{-1}}$ for surface temperatures of 285 K and 308 K respectively. This change is about 1.5 times larger than for ARTS, which changes only 52 % from -1.72 to $-0.82\,\mathrm{Wm^{-2}K^{-1}}$ for the same temperature range. This is caused by an imbalance of the negative lapse-rate feedback and its upper-tropospheric counterpart (WV$\wedge$LR) when using RRTMG. In general, the magnitude of the lapse-rate feedback is only half as large as for the line-by-line calculations.

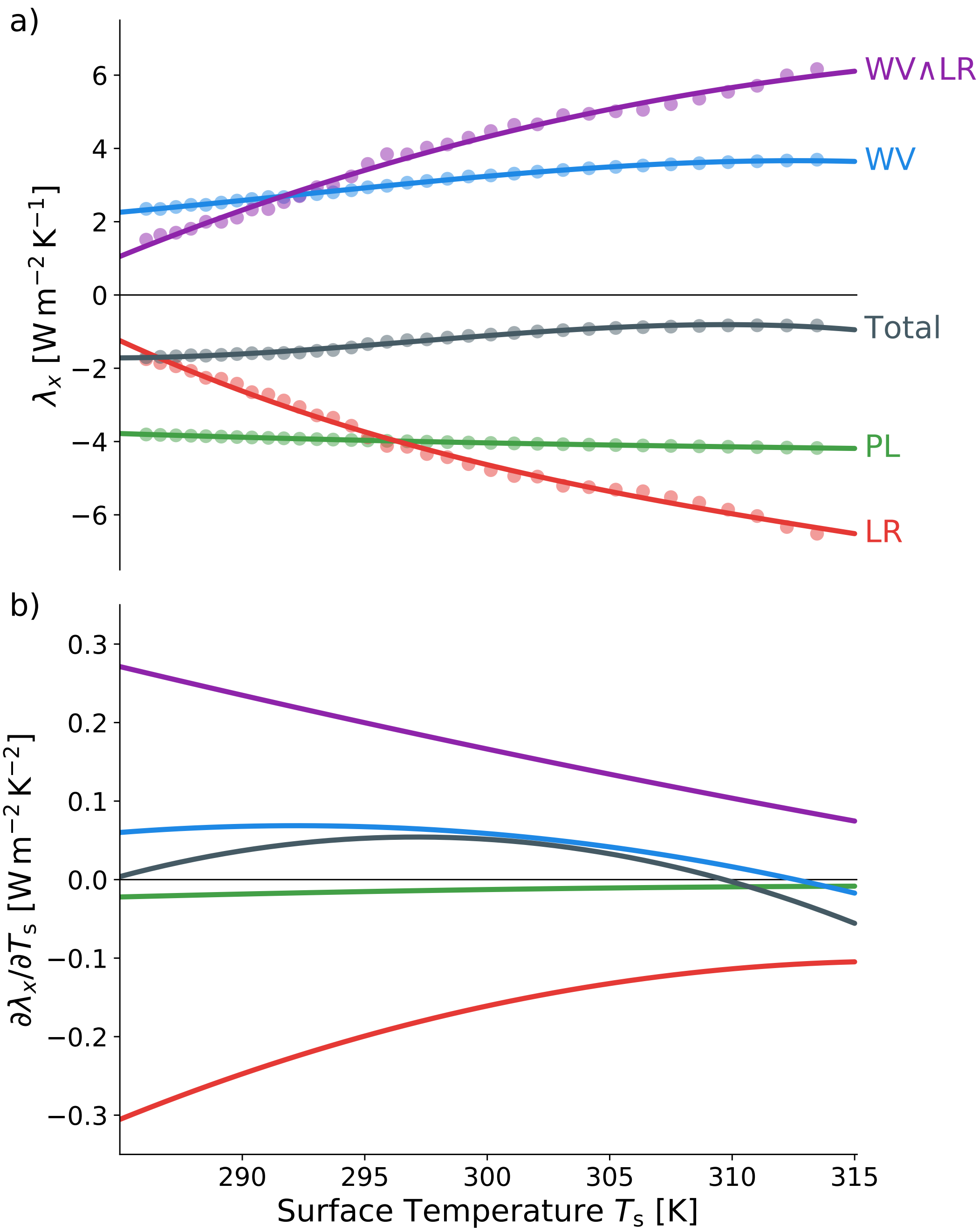

Figure 2. **a)** Decomposed Planck (PL, green), water-vapor (WV, blue), lapse rate (LR, red), combined water-vapor—lapse-rate (WV∧LR, purple), and total feedback (gray) as function of surface temperature. Cubic fits for each data set are plotted as solid lines. **b)** The cubic fits are used to determine the surface-temperature derivative for each feedback individually. Positive values denote surface temperatures at which a radiative feedback increases.

The simulated temperature profile is following the saturated isentropic lapse rate and exceeds the temperature validity range of RRTMG in the upper troposphere for surface temperatures above 308 K (Figure 3b). As a result the pre-calculated lookup tables are out of bounds, which causes errors in the computed radiative fluxes. This threshold is consistent with the surface temperatures at which the radiative feedback decreases again. The modeling studies by Meraner et al. (2013) and Romps (2020) find a decrease in their feedback estimates at 310 K and 308 K respectively, which indicates that they are also exceeding the validity range of RRTMG.

It is worth noting, that RRTMG uses look up tables which are valid for surface temperatures as high as 320 K, but due to the construction of the look up tables at surface temperatures above 308 K the moist-adiabat implies mid- and upper-tropospheric temperatures which are out of bounds, leading to substantial errors. Therefore, when using RRTMG for surface temperatures above 308 K, one has to adapt the underlying lookup tables, as for example done by Popp et al. (2015), or use a different radiative transfer model.

5 Spectral radiative feedbacks

As discussed above, the near-constancy of the total climate feedback at high temperatures is in line with the qualitative model of Ingram (2010). The conceptual model predicts a zero radiative feedback in spectral regions that are both dominated by water vapor and fully opaque. These conditions are fulfilled for a large part of the spectrum at high surface temperatures. Koll and Cronin (2018) find a rapid closing of the atmospheric window at surface temperatures above 300 K, because the abundance of water vapor increases continuum absorption. We want to illuminate the validity of the theoretical model by calculating spectrally resolved radiative feedbacks.

The line-by-line radiative transfer model ARTS is used to simulate two outgoing longwave radiation (OLR) spectra, one after the stratospheric adjustment, and one in equilibrium, which are used to derive the spectral radiative feedback λ_ν:

$$\lambda_\nu = \frac{\Delta E_{\mathrm{OLR}}(\nu)}{\Delta T_{\mathrm{s}}} \tag{6}$$

with change in OLR $\Delta E_{\mathrm{OLR}}(\nu)$ and surface temperature change ΔT_{s}.

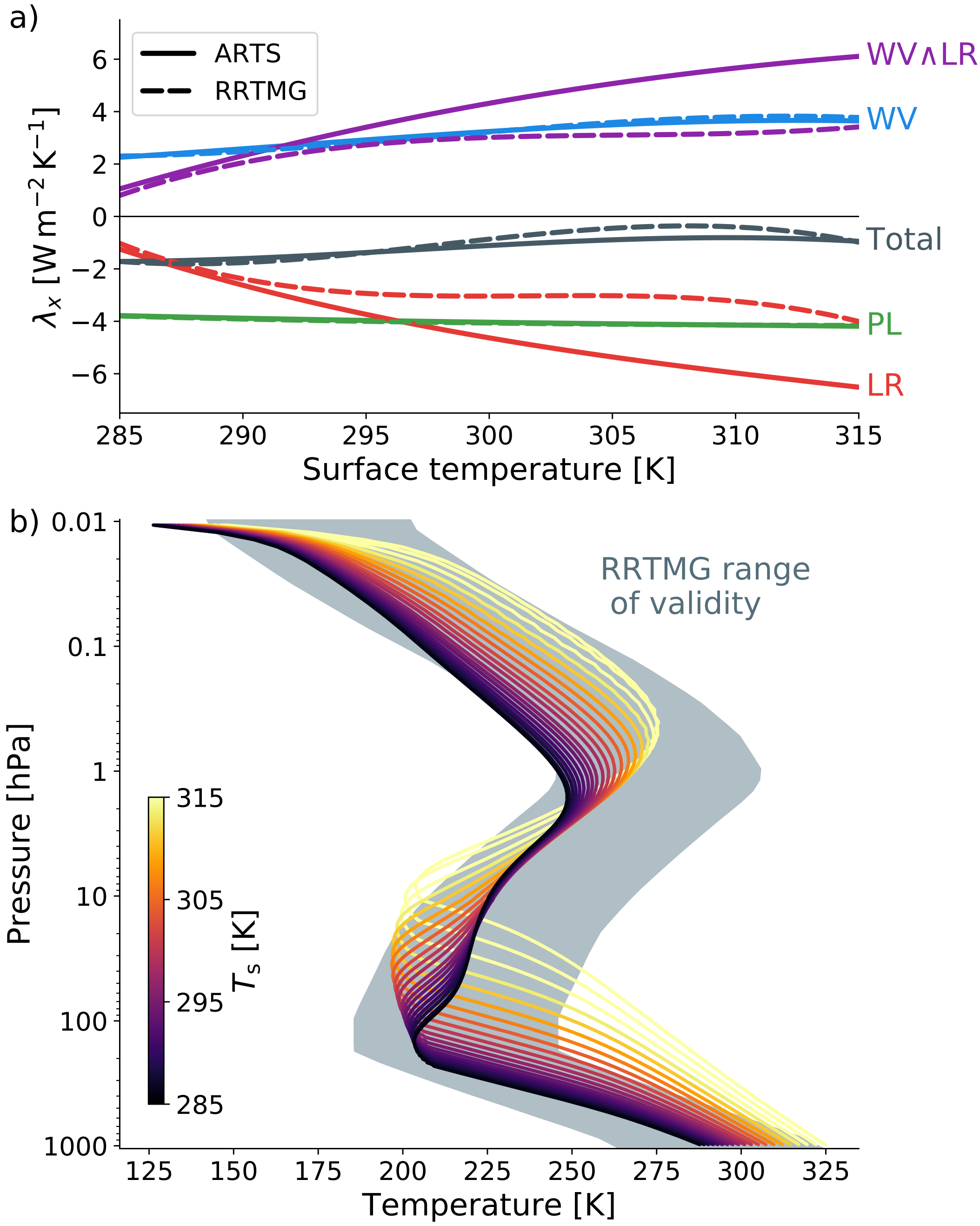

Figure 3. **a)** Decomposed radiative feedbacks as a function of surface temperature. The feedbacks λ_x are shown for simulations using the radiation scheme RRTMG (dashed) as well as the line-by-line model ARTS (solid). **b)** Temperature profiles for different values of surface heat transport (in color) alongside the RRTMG temperature range.

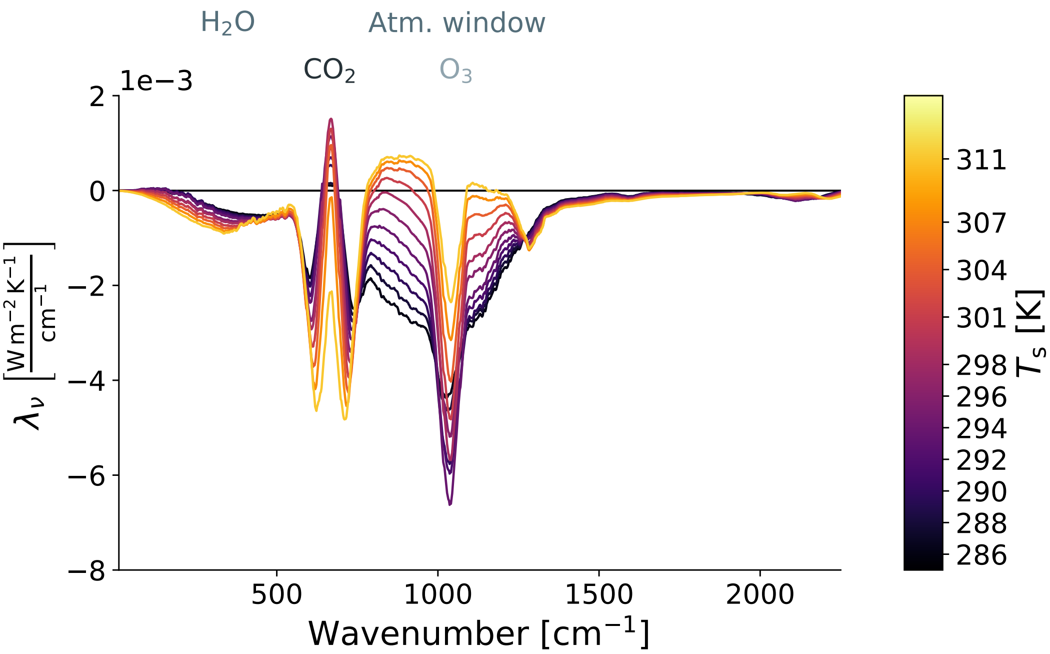

Figure 4. Spectral radiative feedback as a function of wavenumber for different surface temperatures (in colors). The spectra are cut at 2,250 cm^{-1} to better resolve regions of interest. The actual line-by-line simulations cover a wavenumber range from 10–3,250 cm^{-1}.

Figure 4 shows the total spectral feedback as a function of wavenumber ν (see supporting information for decomposed spectral feedbacks). There is a strong temperature-dependence of the spectral feedback in the atmospheric window between 800 and 1000 cm^{-1}, which is mainly driven by increased continuum absorption that shuts the atmospheric window (Koll & Cronin, 2018). As soon as the atmosphere is fully opaque in these spectral regions the radiative feedback is independent of the surface temperature, in agreement with Ingram (2010). The same behavior can be seen in the water-vapor dominated band below 500 cm^{-1}, which is opaque for all simulated surface temperatures.

We find that the total radiative feedback in spectral regions that are mainly dominated by water vapor absorption is indeed close to zero as soon as the atmosphere becomes fully opaque at high temperatures. Hence, our results link the findings of Koll and Cronin (2018) with the theory of Ingram (2010) to explain the temperature-dependence of the total radiative clear-sky feedback for a wide range of surface temperatures.

6 Conclusions

We tune our 1D-RCE model to different surface temperatures by introducing a surface enthalpy sink. We suggest that this is the best approach to analyze state-dependencies of radiative feedbacks in a single-column model.

The longwave radiation scheme used is the line-by-line model ARTS to ensure an accurate computation of radiative fluxes and heating rates over a wide temperature range. By comparison to calculations with the RRTMG radiation scheme, we find that the use of that fast radiation scheme in extreme climates, outside its validity range, lead to false predictions on the state-dependence at high surface temperatures in at least two other modeling studies (e.g. Meraner et al., 2013; Romps, 2020).

The total radiative clear-sky feedback increases from -1.7 to $-0.8\,\mathrm{Wm^{-2}K^{-1}}$ for surface temperatures between 285 and 305 K, which can be attributed to a strengthening of the water-vapor feedback. This strengthening maximizes at surface temperatures of about 297 K at which the atmospheric window closes rapidly due to increased water-vapor continuum absorption.

After the closure of the atmospheric window, corresponding to surface temperatures above 305 K, the total radiative feedback is approximately independent of further surface temperature increases, in agreement with the conceptual model of Ingram (2010).

Acknowledgments

Contains modified Copernicus Climate Change Service Information (ERA5) [2018].

With this work we contribute to the Cluster of Excellence "CLICCS—Climate, Climatic Change, and Society" (EXC 2037, Project Number 390683824), and to the Center for Earth System Research and Sustainability (CEN) of Universität Hamburg.

The model source is developed under the MIT License and available on `github.com/atmtools/konrad`.

References

Becker, T., & Stevens, B. (2014). Climate and climate sensitivity to changing co2 on an idealized land planet. *Journal of Advances in Modeling Earth Systems*, *6*(4), 1205–1223. Retrieved from `https://agupubs.onlinelibrary.wiley.com/doi/abs/10.1002/2014MS000369` doi: 10.1002/2014MS000369

Budyko, M. I. (1969). The effect of solar radiation variations on the climate of the earth. *Tellus*, *21*(5), 611–619. Retrieved from `https://doi.org/10.3402/tellusa.v21i5.10109` doi: 10.3402/tellusa.v21i5.10109

Buehler, S. A., Mendrok, J., Eriksson, P., Perrin, A., Larsson, R., & Lemke, O. (2018). ARTS, the atmospheric radiative transfer simulator — version 2.2, the planetary toolbox edition. *Geoscientific Model Development*, *11*(4), 1537–1556. doi: 10.5194/gmd-11-1537-2018

Colman, R., & McAvaney, B. (2009). Climate feedbacks under a very broad range of forcing. *Geophysical Research Letters*, *36*(1). doi: 10.1029/2008GL036268

Cronin, T. W. (2014). On the choice of average solar zenith angle. *Journal of the Atmospheric Sciences*, *71*(8), 2994–3003. doi: 10.1175/JAS-D-13-0392.1

Cronin, T. W., & Emanuel, K. A. (2013). The climate time scale in the approach to radiative-convective equilibrium. *Journal of Advances in Modeling Earth Systems*, *5*(4), 843–849. Retrieved from `https://agupubs.onlinelibrary.wiley.com/doi/abs/10.1002/jame.20049` doi: 10.1002/jame.20049

Cronin, T. W., & Wing, A. A. (2017). Clouds, circulation, and climate sensitivity in a radiative-convective equilibrium channel model. *Journal of Advances in Modeling Earth Systems*, *9*(8), 2883–2905. doi: 10.1002/2017MS001111

Dacie, S., Kluft, L., Schmidt, H., Stevens, B., Buehler, S. A., Nowack, P. J., … Birner, T. (2019). A 1D RCE study of factors affecting the tropical tropopause layer and surface climate. *Journal of Climate*, *32*(20), 6769–6782. Retrieved from `https://doi.org/10.1175/JCLI-D-18-0778.1` doi: 10.1175/JCLI-D-18-0778.1

Drotos, G., Becker, T., Mauritsen, T., & Stevens, B. (2020). Global variability in radiative-convective equilibrium with a slab ocean under a wide range of co2 concentrations. *Tellus A: Dynamic Meteorology and Oceanography*, *72*(1), 1–19. Retrieved from `https://doi.org/10.1080/16000870.2019.1699387` doi: 10.1080/16000870.2019.1699387

Eriksson, P., Buehler, S. A., Davis, C. P., Emde, C., & Lemke, O. (2011). ARTS, the atmospheric radiative transfer simulator, version 2. *Journal of Quantitative Spectroscopy and Radiative Transfer*, *112*(10), 1551–1558. doi: 10.1016/j.jqsrt.2011.03.001

Gordon, I. E., Rothman, S., Hill, C., Kochanov, R. V., Tan, Y., Bernath, P. F.,

... Zak, E. J. (2017). The HITRAN2016 molecular spectroscopic database. *Journal of Quantitative Spectroscopy and Radiative Transfer*, *203*, 3–69. doi: 10.1016/j.jqsrt.2017.06.038

Gregory, J. M., Ingram, W. J., Palmer, M. A., Jones, G. S., Stott, P. A., Thorpe, R. B., ... Williams, K. D. (2004). A new method for diagnosing radiative forcing and climate sensitivity. *Geophysical Research Letters*, *31*(3), 1–4. doi: 10.1029/2003GL018747

Hohenegger, C., & Stevens, B. (2016). Coupled radiative convective equilibrium simulations with explicit and parameterized convection. *Journal of Advances in Modeling Earth Systems*, *8*(3), 1468–1482. Retrieved from `https://agupubs.onlinelibrary.wiley.com/doi/abs/10.1002/2016MS000666` doi: 10.1002/2016MS000666

Ingram, W. (2010). A very simple model for the water vapour feedback on climate change. *Quarterly Journal of the Royal Meteorological Society*, *136*(646), 30–40. doi: 10.1002/qj.546

Kluft, L., & Dacie, S. (2020, June). *atmtools/konrad: Add line-by-line radiation and conceptual clouds.* Zenodo. Retrieved from `https://doi.org/10.5281/zenodo.3899702` doi: 10.5281/zenodo.3899702

Kluft, L., Dacie, S., Buehler, S. A., Schmidt, H., & Stevens, B. (2019). Re-examining the first climate models: Climate sensitivity of a modern radiative-convective equilibrium model. *Journal of Climate*, *32*(23), 8111–8125. doi: 10.1175/JCLI-D-18-0774.1

Koll, D. D. B., & Cronin, T. W. (2018). Earth's outgoing longwave radiation linear due to h2o greenhouse effect. *Proceedings of the National Academy of Sciences*, *115*(41), 10293–10298. doi: 10.1073/pnas.1809868115

Manabe, S., & Stouffer, R. J. (1980). Sensitivity of a global climate model to an increase of co2 concentration in the atmosphere. *Journal of Geophysical Research: Oceans*, *85*(C10), 55290–5554. doi: 10.1029/JC085iC10p05529

Meraner, K., Mauritsen, T., & Voigt, A. (2013). Robust increase in equilibrium climate sensitivity under global warming. *Geophysical Research Letters*, *40*(22), 5944–5948. doi: 10.1002/2013GL058118

Minschwaner, K., & Dessler, A. E. (2004). Water vapor feedback in the tropical upper troposphere: Model results and observations. *Journal of Climate*, *17*, 1272–1282. doi: 10.1175/1520-0442(2004)017⟨1272:WVFITT⟩2.0.CO;2

Mlawer, E. J., Payne, V. H., Moncet, J.-L., Delamere, J. S., Alvarado1, M. J., & Tobin, D. C. (2012). Development and recent evaluation of the MT_CKD model of continuum absorption. *Philosophical Transactions of the Royal Society A*, *370*(1968), 2520–2556. doi: 10.1098/rsta.2011.0295

Mlawer, E. J., Taubman, S. J., Brown, P. D., Iacono, M. J., & Clough, S. A. (1997). Radiative transfer for inhomogeneous atmospheres: RRTM, a validated correlated-k model for the longwave. *Journal of Geophysical Research*, *102*, 16663–16682.

Niiler, P. P. (1992). The ocean circulation. In K. E. Trenberth (Ed.), *Climate system modeling* (chap. 4). Cambridge University Press.

Popke, D., Stevens, B., & Voigt, A. (2013). Climate and climate change in a radiative-convective equilibrium version of echam6. *Journal of Advances in Modeling Earth Systems*, *5*(1), 1–14. doi: 10.1029/2012MS000191

Popp, M., Schmidt, H., & Marotzke, J. (2015, 01). Initiation of a runaway greenhouse in a cloudy column. *Journal of the Atmospheric Sciences*, *72*(1), 452–471. Retrieved from `https://doi.org/10.1175/JAS-D-13-047.1`

Romps, D. M. (2020). Climate sensitivity and the direct effect of carbon dioxide in a limited-area cloud-resolving model. *Journal of Climate*, *33*(9), 3413–3429. Retrieved from `https://doi.org/10.1175/JCLI-D-19-0682.1` doi: 10.1175/JCLI-D-19-0682.1

Wing, A. A., Reed, K. A., Satoh, M., Stevens, B., Bony, S., & Ohno, T. (2017). Radiative-convective equilibrium model intercomparison project. *Geoscientific Model Development Discussions*, *2017*, 1–34. doi: 10.5194/gmd-2017-213